ABSTRACT

SUBSIDENCE CAUSED BY AN UNDERGROUND NUCLEAR EXPLOSION

by

W. W. Hakala

An underground nuclear detonation creates a cavity, which may be followed by the formation of a rubble chimney and possibly by a surface subsidence crater. A knowledge of the mechanisms of surface and subsurface subsidence is valuable not only because of the potential engineering uses of the chimneys and craters that may form, but also for the prevention of surface damage.

Some of the parameters that are of interest in the subsidence phenomenon are the height and volume of the chimney, the porosity of the chimney, the crater size (depth and radius) and shape, and the time required after detonation for formation of the chimney or crater. The influence of the properties of the subsidence medium on the geometry of the subsidence crater must be considered. The conditions under which partial or complete subsidence is prevented must also be studied.

The applicability of the relations that have been developed for the flow of bulk solids for relatively small masses and low pressures to the subsidence problem associated with nuclear explosions is examined. Rational modifications are made to describe the subsidence problem. Sensitivity of the subsidence parameters to material properties and the prevailing geometry is shown. Comparison with observed results at the Nevada Test Site is made and the variations encountered are found to be within reasonable limits.

The chimney size and subsidence crater dimensions are found to be a function of the bulking characteristics of the medium, the strength parameters, the dimensions of the subsurface cavity, and the depth of the cavity. The great influence of the strength parameters on the collapse times is shown. For a given medium, the prevention of subsidence is dependent on the cavity size.

SUBSIDENCE CAUSED BY AN UNDERGROUND NUCLEAR EXPLOSION

W. W. Hakala, Deputy Director for Engineering

Environmental Research Corporation
Alexandria, Virginia

The utility of subsidence craters for engineering purposes is questionable, since greater efficiency in producing surface depressions can be obtained with ejecta craters. Still, if containment of radioactivity is mandatory, subsidence craters may provide a solution for certain problems. Subsurface subsidence (e.g., permeable chimneys) does have immediate application in the Plowshare program. Independent of the engineering applications, it is necessary to determine the extent of surface subsidence for safety reasons. A knowledge of the subsidence mechanisms may even permit the control of subsidence to some degree.

This paper is a study of the subsidence associated with the collapse of underground spherical cavities (which were produced by underground nuclear detonations). The results are based on the work of Jenike and his colleagues, who have developed many of the concepts for the flow of bulk solids (bin-flow theory). Homogeneity, isotropy, and steady-state flow are usually assumed in Jenike's work.

Although deviations from homogeneity and isotropy are present in most of the subsidence cases, it is assumed that these effects are small. Of course, the presence of layered earth media having widely varying strength properties would affect the results significantly, and would require individual consideration.

In contrast to the fixed outlet dimensions in bin-flow theory, the material adjacent to the assumed spherical cavity is subject to collapse. However, it is assumed that the flow boundaries are close to the cavity walls and thus the outlet dimensions can be expressed in terms of the cavity radius, R_c.

This work also requires the cavity pressure to be approximately atmospheric. While the time to collapse will be dependent on the cavity pressure, it is not believed that the potential flow patterns will be affected significantly by this assumption. Because the type of subsidence being considered may involve vertical

movements of several hundred feet, it is quite likely that the steady-state flow patterns are reached in many instances.

The stresses and dimensions used in bin-flow theory are approximately two orders of magnitude less than those in the subsidence problem. However, the fundamental relations (equilibrium equations and yield criterion) remain valid.

A large portion of Jenike's work is concerned with the shape of the yield surface at small compressive stresses. Variations in the yield surface caused by consolidating pressures, temperatures, moisture, and time have been carefully examined, and a corresponding vocabulary of bulk solids flow has been developed. Jenike (1961) has provided strong physical arguments for a curved yield surface at small stress values. Because of the assumptions, the large pressures, and a lack of known material properties (in general), the present study does not warrant such refinement. Therefore, the linear Mohr-Coulomb yield criterion is assumed. Bin-flow theory is applied directly, if applicable, or modified to represent the physical situation.

THEORY OF SUBSIDENCE

Yield Criteria

Most of the stresses and strains encountered in the subsidence problem are compressive. Thus, it is convenient to assume compressive values as being positive and tension values as being negative. The collapsing medium has both cohesion (c) and internal friction (ϕ), and for purposes of analyses, is also assumed to be homogeneous, isotropic, and compressible.

The selection of the Mohr-Coulomb yield criterion as the failure mechanism requires only a knowledge of the major and minor principal stresses (σ_1 and σ_3, respectively), and is independent of the intermediate principal stress (σ_2). Recent experimental work has found that the intermediate principal stress does affect the stress values at failure to a certain degree. However, this effect is quite small and will be neglected in this discussion. (it can also be argued that the selection of an angle of internal friction, ϕ, has taken into account the effect of σ_2.)

The yield surface corresponding to the Mohr-Coulomb hypothesis in the principal stress space is shown in Figure 1. Neglecting the effect of σ_2 on yield results in a yield surface with sharp corners, which seems to violate one's intuition of expecting smooth transitions in physical processes. However, the rate of change of curvature at the edges is very large and thus the yield surface can be represented by a pyramid.

The usually assumed "open" yield surface used in soil mechanics was modified by Jenike and Shield (1959) to agree with the concept of normality and physical observations. This modification is the addition of a base that is perpendicular to the line equally inclined to each of the three principal stress axes. The position of the base depends on the mean stress, $\sigma'_m = (\sigma_1 + \sigma_2 + \sigma_3)/3$, during flow.

The concept of normality requires that the strain-rate vector ($\dot{\epsilon}$) be perpendicular to the yield surface. Inclusion of a base not only permits compression under a hydrostatic stress, but also allows either expansion or contraction if the stress state corresponds to a corner of the base, e.g., point "A" (the corresponding strains being plotted on the same axes as the stress). This model, then agrees with physical observations that either expansion or contraction takes place during flow. For failure stress states corresponding to points on the faces or edges of the pyramid, the normality requirement dictates material expansion.

Jenike (1961) found from laboratory tests on numerous materials that during "flow" (after incipient failure) the ratio of the principal stresses remains constant for a given material. The significance of this finding can be seen in a normal stress (σ) vs. shear stress (τ) plot (Figure 2). From the geometry it is readily seen that

$$\frac{\sigma_1}{\sigma_3} = \frac{1 + \sin \delta}{1 - \sin \delta} \quad , \qquad (1)$$

where δ is called the effective angle of friction. The envelope to the stress circles is called the effective yield locus (EYL). Because the stress circles at failure must also be tangent to the yield surface (or the yield locus, YL in Figure 2), it is then necessary for the yield surface to change in size as the principal stresses vary in the flowing medium (unless the yield locus coincides with the effective yield locus, i.e., no cohesive strength).

The linear Mohr-Coulomb yield locus together with a stress circle at failure are given in Figure 3. It is apparent from the geometry that the angle between the failure planes and the direction of the major principal stress is

$$\mu = 45° - \phi/2 \quad . \qquad (2)$$

The locus of points (in a plane) lying on the failure planes are called sliplines.

For the axially symmetric subsidence problem, it is convenient to work in the meridian plane and use either rectangular

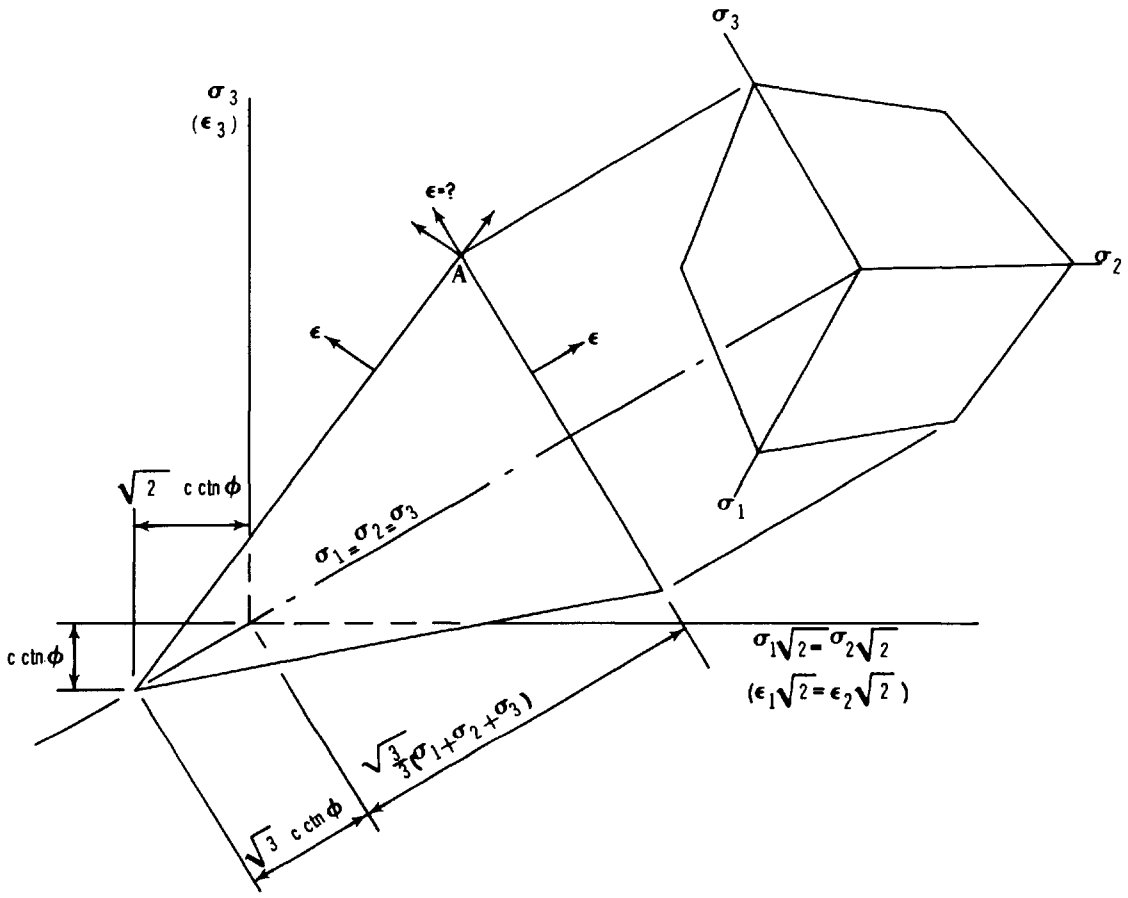

FIGURE 1. YIELD SURFACE IN PRINCIPAL STRESS SPACE

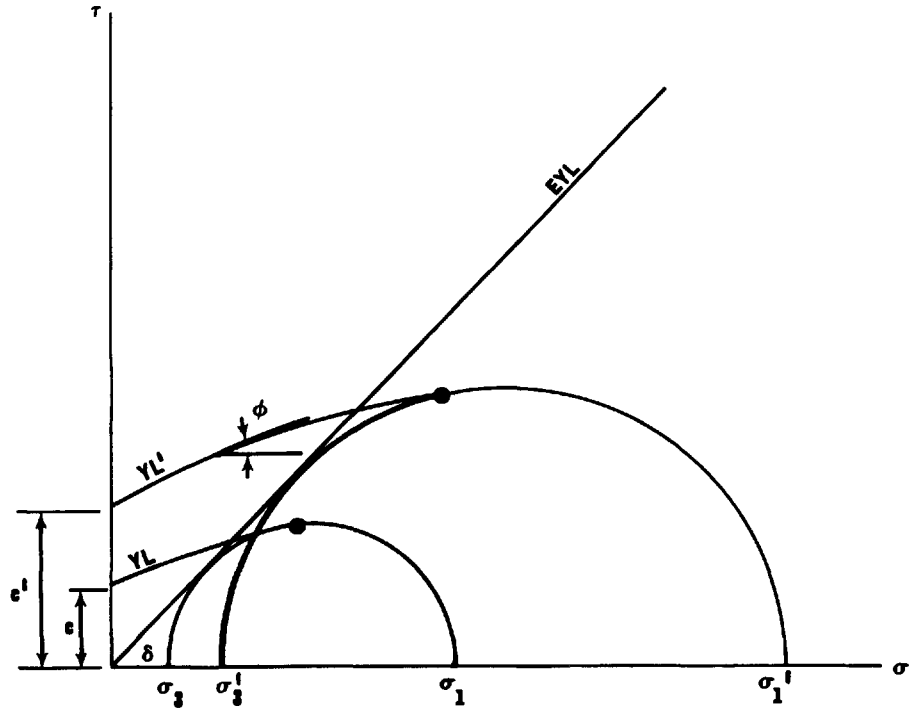

FIGURE 2. CHANGE OF YIELD LOCUS (YL) WITH CONSOLIDATION PRESSURE

or polar (or spherical) coordinates. Figure 4 shows these coordinate systems in the meridian plane.

The yield criterion in Figure 3 can be expressed as

$$\frac{1}{4}(\sigma_r-\sigma_\theta)^2 + \tau_{r\theta}^2 = \frac{\sin^2\phi}{4}(\sigma_r+\sigma_\theta+2\psi)^2 \quad , \qquad (3a)$$

or

$$\frac{1}{4}(\sigma_x-\sigma_y)^2 + \tau_{xy}^2 = \frac{\sin^2\phi}{4}(\sigma_x+\sigma_y+2\psi)^2 \quad , \qquad (3b)$$

where ψ = c ctn ϕ.

Fundamental Relations

The two non-trivial differential equations of equilibrium for the stress state shown in Figure 5 expressed in spherical coordinates are (Sokolnikoff, 1956):

$$\begin{aligned} &\frac{\partial\sigma_r}{\partial r} + \frac{1}{r}\frac{\partial\tau_{r\theta}}{\partial\theta} + \frac{1}{r}\left[2\sigma_r-\sigma_\theta-\sigma_\alpha+\tau_{r\theta}\,\mathrm{ctn}\theta\right] + \gamma\cos\theta = 0 \quad , \\ &\frac{\partial\tau_{r\theta}}{\partial r} + \frac{1}{r}\frac{\partial\sigma_\theta}{\partial\theta} + \frac{1}{r}\left[(\sigma_\theta-\sigma_\alpha)\mathrm{ctn}\theta+3\tau_{r\theta}\right] - \gamma\sin\theta = 0 \quad , \end{aligned} \qquad (4a)$$

where

$\sigma_r, \sigma_\theta, \sigma_\alpha, \tau_{r\theta}$ = stress components

r, θ, α = spherical coordinates

γ = density of medium.

If expressed in rectangular coordinates.....

$$\begin{aligned} &\frac{\partial\sigma_x}{\partial x} + \frac{\partial\tau_{xy}}{\partial y} + \frac{\tau_{xy}}{y} = \gamma \\ &\frac{\partial\tau_{xy}}{\partial x} + \frac{\partial\sigma_y}{\partial y} + \frac{\sigma_y-\sigma_\alpha}{y} = 0 \quad . \end{aligned} \qquad (4b)$$

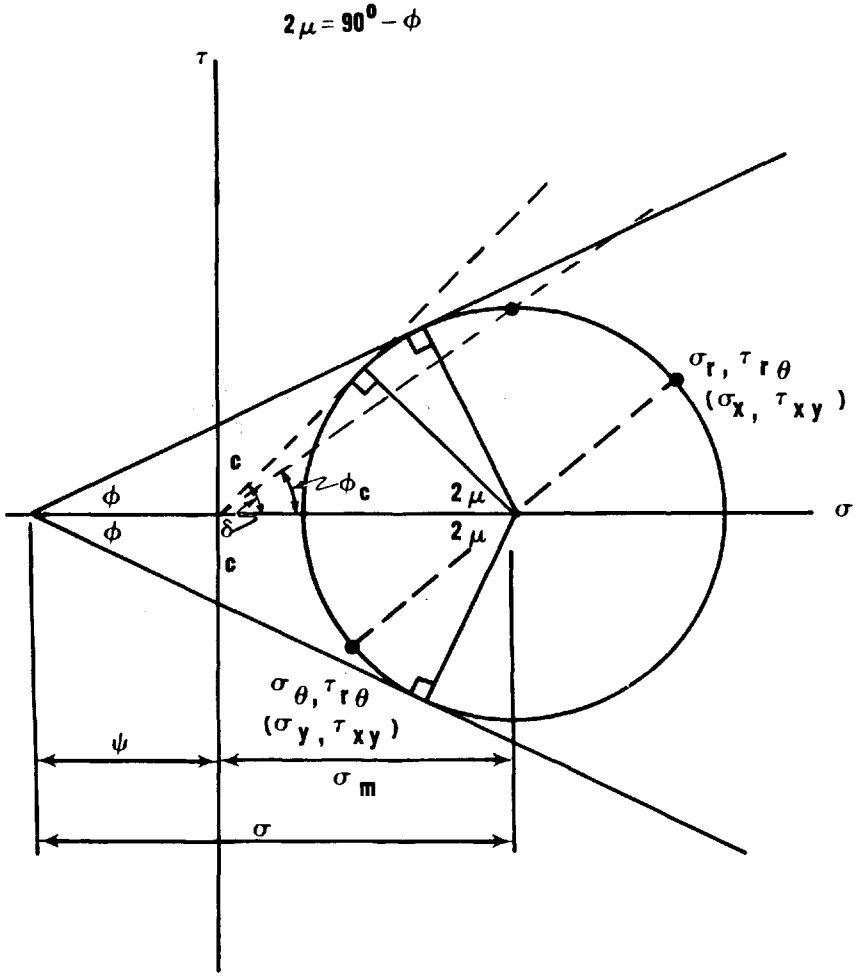

FIGURE 3. MOHR–COULOMB YIELD CRITERION

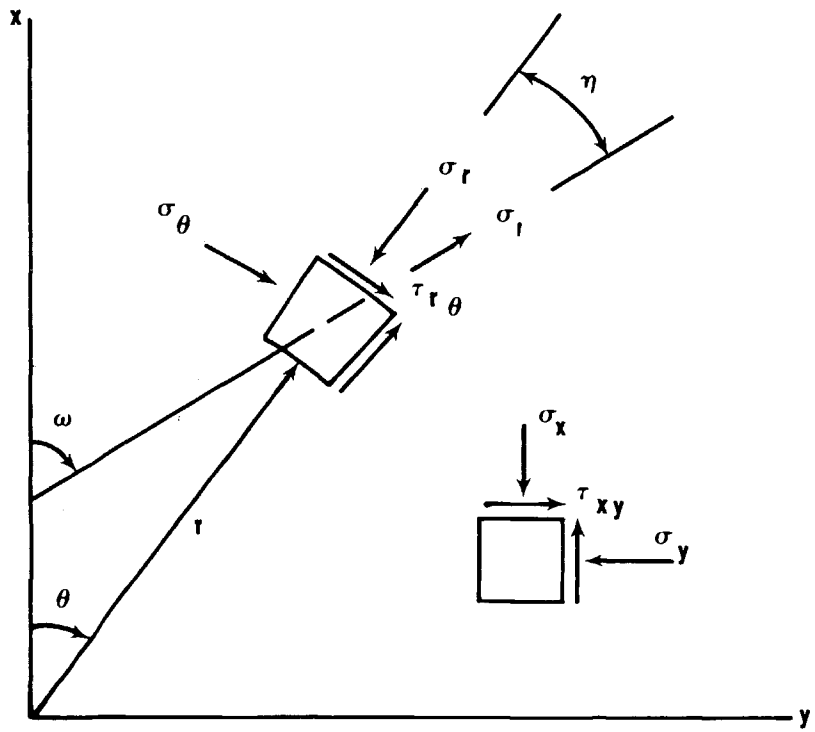

FIGURE 4. COORDINATE SYSTEMS IN MERIDIAN PLANE

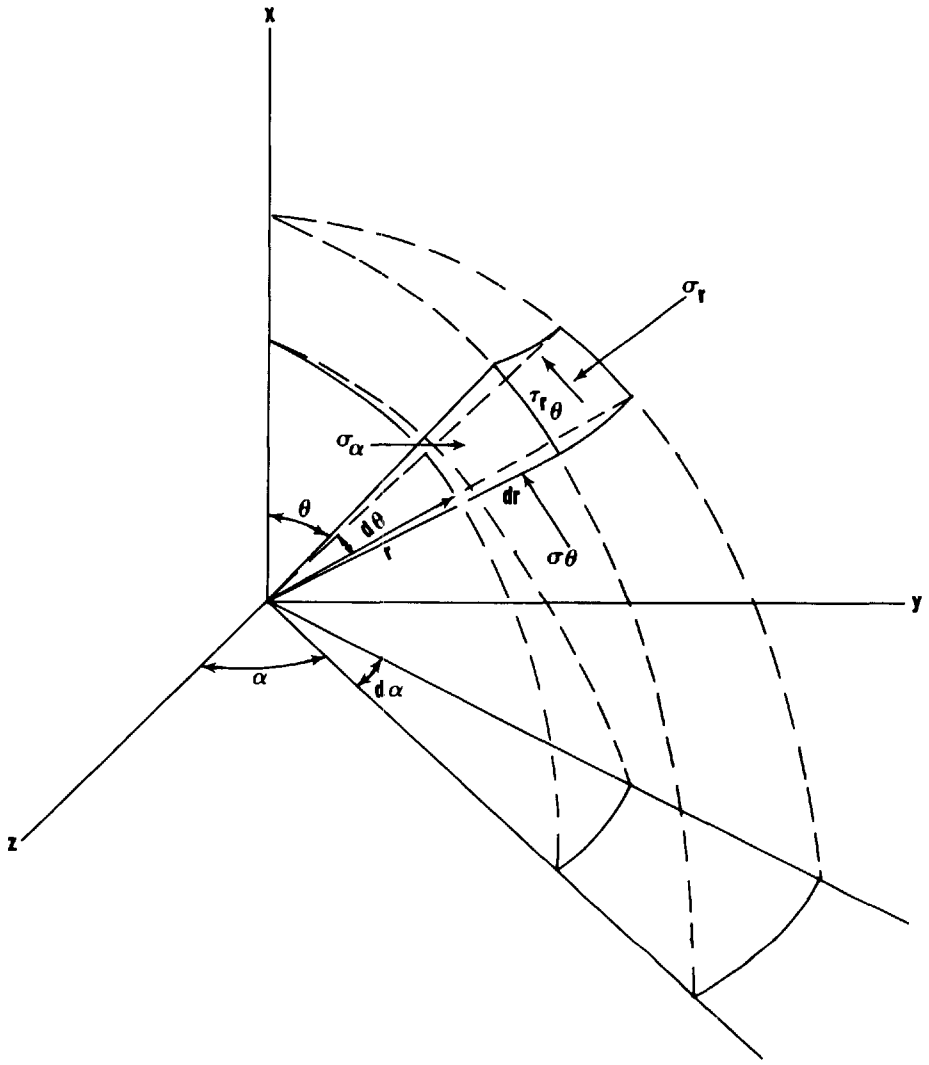

FIGURE 5. EQUILIBRIUM OF AN ELEMENT IN AXIALLY SYMMETRIC FLOW (SPHERICAL COORDINATES)

Assuming that every point in the collapsing material is in a state of limiting equilibrium, relations (3) and (4) provide three equations containing five unknowns (σ_r, σ_θ, σ_α, τ_{xy}, γ). During flow of bulk solids, Jenike (1961) found by experiment that the density could be expressed as a function of the mean stress in the meridian plane, $\sigma_m = (\sigma_r + \sigma_\theta)/2 = (\sigma_x + \sigma_y)/2$, i.e.,

$$\gamma = \gamma_o(1 + \sigma_m)^\beta \qquad (5a)$$

where γ_o and β are constants for a given material. If σ_m is expressed in pounds per square foot (psf), then Jenike found that β did not exceed .10 for any material that he tested. One would anticipate greater density changes than this for media containing large blocks. However, it can still be assumed that γ is a function of the mean stress, i.e.,

$$\gamma = \gamma_o\, f(\sigma_m) \quad . \qquad (5b)$$

The remaining relation is found from the Haar-von Karman hypothesis, which states that the circumferential stress, σ_α, is equal to the major principal stress in converging flow,

$$\sigma_\alpha = \sigma_1 \quad \text{(converging flow)}, \qquad (6a)$$

and the equal to the minor principal stress in diverging flow,

$$\sigma_\alpha = \sigma_3 \quad \text{(diverging flow)} \quad . \qquad (6b)$$

Subject to the boundary conditions, it is theoretically possible to solve the subsidence problem from relations (3), (4), (5), and (6). The number of variables in these relations can be reduced by the substitution

$$\sigma = \psi + \sigma_m \quad . \qquad (7)$$

If ω is the angle between the vertical axes and the direction of the major principal stress (Figure 4), the stresses at failure can be expressed as (see Figure 3)

$$\sigma_x = \sigma(1+\sin\phi\cos2\omega) - \psi \quad ,$$

$$\sigma_y = \sigma(1-\sin\phi\cos2\omega) - \psi \quad ,$$

$$\sigma_\alpha = \sigma(1+\sin\phi) - \psi \quad , \tag{8}$$

$$\tau_{xy} = \sigma\sin\phi\sin2\omega \quad .$$

Replacement of ω by η resultsin similar relations for σ_r, σ_θ, and $\tau_{r\theta}$ (see Figure 4).

Characteristics

The stress characteristics (lines along which an infinity of solutions are possible) can be found by substituting equations (8) into (4b):

$$(1+\sin\phi\cos2\omega)\frac{\partial\sigma}{\partial x} + \sin\phi\sin2\omega\frac{\partial\sigma}{\partial y} - 2\sigma\sin\phi\sin2\omega\frac{\partial\omega}{\partial x}$$

$$+2\sigma\sin\phi\sin2\omega\frac{\partial\omega}{\partial y} = \gamma - \frac{\sigma}{y}\sin\phi\sin2\omega \quad ,$$

$$\sin\phi\sin2\omega\frac{\partial\sigma}{\partial x} + (1-\sin\phi\cos2\omega)\frac{\partial\sigma}{\partial y} + 2\sigma\sin\phi\cos2\omega\frac{\partial\omega}{\partial x} \tag{9}$$

$$+2\sigma\sin\phi\sin2\omega\frac{\partial\omega}{\partial y} = \frac{\sigma}{y}\sin\phi(1+\cos2\omega) \quad .$$

Sokolovsky (1960) found it convenient to define the quantity

$$S = \frac{\operatorname{ctn}\phi}{2}\ln\frac{\sigma}{\sigma_o} \quad , \tag{10}$$

where σ_o is an arbitrary stress. Therefore,

$$\frac{\partial\sigma}{\partial x} = 2\sigma\tan\phi\frac{\partial S}{\partial x} \quad ,$$

$$\frac{\partial\sigma}{\partial y} = 2\sigma\tan\phi\frac{\partial S}{\partial y} \quad . \tag{11}$$

After replacement in equations (9) and some algebraic and trigonometric manipulations, the equilibrium equations become

$$\frac{\partial(S+\omega)}{\partial x} + \frac{\partial(S+\omega)}{\partial y}\tan(\omega+\mu) = A \quad ,$$

$$\frac{\partial(S-\omega)}{\partial x} + \frac{\partial(S-\omega)}{\partial y}\tan(\omega-\mu) = B \quad , \qquad (12)$$

where

$$A = \frac{\gamma\sin(\omega-\mu)}{2\sigma\sin\phi\cos(\omega+\mu)} + \frac{\cos(\omega+u)+\cos(\omega-\mu)}{2y\cos(\omega+\mu)} \quad ,$$

$$B = \frac{\gamma\sin(\omega+\mu)}{2\sigma\sin\phi\cos(\omega-\mu)} \quad \frac{\cos(\omega-\mu)+\cos(\omega+\mu)}{2y\cos(\omega-\mu)} \quad .$$

Since

$$d(S\pm\omega) = \frac{\partial(S\pm\omega)}{\partial x}\,dx + \frac{\partial(S\pm\omega)}{\partial y}\,dy \quad , \qquad (13)$$

the four equations [(12), (13)] can be solved for the derivatives, $\partial(S\pm\omega)/\partial x$, $\partial(S\pm\omega)/\partial y$. It is found that these derivatives have an infinity of solutions when

$$\frac{dy}{dx} = \tan(\omega\pm\mu) \quad , \qquad (14)$$

and the two families of curves defined by these slopes are called the stress characteristics. Thus, the stress characteristics coincide with the sliplines for incipient failure (see Figure 4).

During flow (assuming the validity of equation (1)) the stress characteristics have the slopes,

$$\frac{dy}{dx} = \tan\left[\omega\pm(45-\delta/2)\right] \quad , \qquad (15)$$

and, in general, do not coincide with the sliplines.

The velocity field for steady flow is also found by determining its characteristics. If u and v are the velocity components in the x and y directions, respectively, the continuity equation for axi-symmetric flow becomes

$$\frac{\partial}{\partial x}(\gamma\, u\, y) + \frac{\partial}{\partial y}(\gamma\, v\, y) = 0 \quad . \qquad (16)$$

After differentiating,

$$\frac{\partial u}{\partial x} + \frac{\partial v}{\partial y} + \frac{v}{y} + \frac{1}{\gamma}\left(u\frac{\partial \gamma}{\partial x} + v\frac{\partial \gamma}{\partial y}\right) = 0 \quad . \qquad (17)$$

Assuming the collapsing medium to be isotropic requires that the directions of the principal strain rates coincide with those of the principal stresses. Since the normal strain rates (ϵ_x, ϵ_y) and the shear strain rates (ϵ_{xy}) are given by

$$\epsilon_x = \frac{\partial u}{\partial x}\ ,\ \epsilon_y = \frac{\partial v}{\partial y}\ ,\ \epsilon_{xy} = \frac{\partial u}{\partial y} + \frac{\partial v}{\partial x} \quad , \qquad (18)$$

then

$$\tan 2\omega = \frac{\frac{\partial u}{\partial y} + \frac{\partial v}{\partial x}}{\frac{\partial u}{\partial x} - \frac{\partial v}{\partial y}} \quad . \qquad (19)$$

Equations (17) and (19) together with the total differentials du and dv, are solved for the derivatives, $\partial u/\partial x, \partial u/\partial y, \partial v/\partial x, \partial v/\partial y$. It is found that the characteristic directions are defined by the slopes

$$\frac{dy}{dx} = \tan(\omega \pm 45°) \quad . \qquad (20)$$

The velocity characteristics are orthogonal and coincide with the stress characteristics only if ϕ or $\delta = 0$. Coincidence with the sliplines occurs only when $\phi = 0$.

The above analyses show that the stress field can be computed independently of the velocity field.

Because of the isotropic requirement, the lines of maximum shear strain rate coincide with velocity characteristics. Physical conditions dictate that a line of infinite shear strain rate is possible only if the cohesion and internal friction are fully mobilized. Thus, lines of infinite shear strain rates must coincide with the sliplines. These lines are referred to as velocity discontinuities. A velocity discontinuity also includes jumps in the velocity magnitude.

The continuity equation in spherical coordinates is

$$\frac{\partial}{\partial r}\left[\gamma\, u_r\, r(r \sin\theta)\right] + \frac{\partial}{\partial \theta}\left[\gamma\, u_\theta (r \sin\theta)\right] = 0 \quad , \qquad (21)$$

while the isotropic condition is

$$\tan 2\eta(r,\theta) = \frac{\dfrac{\partial u_r}{r\partial\theta} + \dfrac{\partial u_\theta}{\partial r} - \dfrac{u_\theta}{r}}{\dfrac{\partial u_r}{\partial r} - \dfrac{u_r}{r} - \dfrac{\partial u_\theta}{r\partial\theta}} \quad . \qquad (22)$$

For radial flow, $u_\theta = 0$, and the equations above reduce to:

$$r\,\frac{\partial u_r}{\partial r} + \left(2 + \frac{r}{\gamma}\cdot\frac{\partial \gamma}{\partial r}\right)u_r = 0 \quad , \qquad (23)$$

$$\frac{\partial u_r}{\partial \theta} + \left(-r\,\frac{\partial u_r}{\partial r} + u_r\right)\tan 2\eta = 0 \quad . \qquad (24)$$

Jenike (1961) has shown that the solution to these equations requires that η be only a function of θ, i.e.,

$$\eta = \eta\,(\theta) \quad . \qquad (25)$$

Jenike has also shown that the radial velocity is zero and the rate of change of velocity with respect to θ is zero or infinite when $\eta = \pi/4,\ 3\pi/4$. Thus it is unlikely that a flow channel will develop beyond these limits. Observations of flow seem to verify this hypothesis. These limits happen to be velocity characteristics.

Radial Stress Fields

The equilibrium equations (4a) in spherical coordinates are useful in examining the stress state. Assuming the origin at the vertex of a converging flow channel, Jenike (1961) assumes that the mean stress (during flow, $\sigma_m = \sigma$) can be expressed as

$$\sigma = r\,\gamma(r,\theta)\,s(r,\theta). \qquad (26)$$

Because a variable density has little influence on the results, $\gamma = \gamma_o$. Using analytical arguments and experimental observations of flow, Jenike finds that s is independent of r. Thus,

$$\sigma = r\ \gamma_o\ s(\theta) \quad . \tag{27}$$

This result means that σ is linearly proportional to r along a ray from the vertex. This is called a radial stress field since it is compatible with a radial velocity field.

It is obvious that equation (27) is not valid up to a stress-free boundary. However, Johanson (1964) has shown that this stress field is valid to the near vicinity of such a boundary.

The limits placed on the boundaries of the flow channel by the radial velocity field require the walls of the channel to be both a velocity characteristic and a slipline. This requires that the wall yield locus pass through the point of maximum shear stress (see Figure 3). Therefore, the angle of friction at the wall (ϕ_c) must be lower than the effective angle of friction (δ), or (see Figure 3)

$$\tan \phi_c = \sin \delta \quad . \tag{28}$$

From numerical solutions of the stress and velocity fields, Jenike found that the angle of the flow channel cannot exceed the values in Table I.

TABLE I

δ	=	30°	40°	50°	60°	70°
Max. θ_c	=	15°	8.1°	4.4°	2.2°	0.5°

The values of δ in this table cover the normal range encountered in bulk solids.

Arching or Doming

Jenike and Leser (1963) determined the lower bound for the dimensions of an outlet opening that would prevent the formation

of a stable dome in the flow channel. This "critical" opening size, expressed in terms of the cavity radius, R_c, is given by

$$(R_c)_d = J(\theta_c)\ C_o/2\gamma \quad , \tag{29}$$

where C_o is the unconfined compressive strength of the medium, and $J(\theta_c)$ depends upon the angle of the flow channel. For the limits of the flow angle given in Table I, $J(\theta_c)$ varies from 2.00 to 2.25 (for circular outlets). Within the limits of the approximations,

$$(R_c)_d \cong C_o/\gamma \quad . \tag{30}$$

Piping or Chimneying

A common occurrence in the flow of bulk solids is for a vertical cylinder (or well) to develop within the material, a phenomenon known as "piping." Jenike and Yen (1963) have performed an analysis similar to that for doming, resulting in the relation (the symbols modified for the subsidence problems)

$$(R_c)_p = C_o M(\phi)/2\gamma \quad , \tag{31}$$

where

$(R_c)_p$ = minimum cavity radius to prevent piping,

$M(\phi)$ = piping function.

For the typical range of ϕ values, equation (31) takes the range of values

$$(R_c)_p \cong (1.2 \text{ to } 6)\ C_o/\gamma \quad . \tag{32}$$

Comparison of equations (30) and (32) shows that, for most values of ϕ, if the cavity radius is large enough to prevent piping, then doming will not occur.

In a homogeneous material, one then might anticipate that for very small cavity radii (i.e., $R_c < \sim C_o/\gamma$) no subsidence crater would form. With increasing cavity radius, a transition zone in which piping or "normal" flow may exist is reached. A range in

slope angles might be expected. At cavity radii larger than that given in equation (32), the slope should reach a constant value.

Excessive Bulking

In geologic materials where doming does not take place, surface subsidence may still be prevented if the material increases in volume upon collapse (bulks) so that the volume of the cavity is accounted for before the chimney propagates to the surface. The ratio of the bulked volume to the initial volume is called the bulking factor, N. It was shown by Berry and Hakala* that the maximum height to which a conically-shaped chimney will rise (H) can be found from the cubic equation (see Figure 6):

$$\left(\frac{R_c}{H}\right)^3 - \frac{3}{2}\frac{N-1}{N+1}\left(\frac{R_c}{H}\right)^2 - \frac{N-1}{N+1}\tan\theta_c\left(\frac{R_c}{H}\right) - \frac{1}{2}\frac{N-1}{N+1}\tan^2\theta_c = 0 \quad . \qquad (33)$$

This equation is valid for (1) H < depth of burial, DOB, if $\theta_c \geq 0$, and (2) $R_c/H > R_c/DOB > -\tan\theta_c$ if $\theta_c < 0$.

Subject to these inequalities, the maximum chimney height results when θ_c is negative. However, for most contained explosions, θ_c algebraically must be larger than about -8° in order for the chimney to reach the surface.

For a vertical flow channel (i.e., $\theta_c = 0°$), the expression (33) reduces to the simple relation (horizontal chimney top)

$$\frac{R_c}{H} = \frac{3}{2}\left(\frac{N-1}{N+1}\right) \quad , \qquad (34)$$

or

$$H = \frac{2}{3}\left(\frac{N+1}{N-1}\right)(R_c) \quad . \qquad (35)$$

The bulking factor (N) is not a constant for a given material, but depends on the initial porosity of the medium, the particle size produced during the initial yielding, and probably the energy absorbed by the solids during collapse. In general, the bulking factors for rock will be much larger than for soil. This is due

*This work is contained in a classified report to the U.S. Atomic Energy Commission and is available to those with the proper access clearance and a need to know.

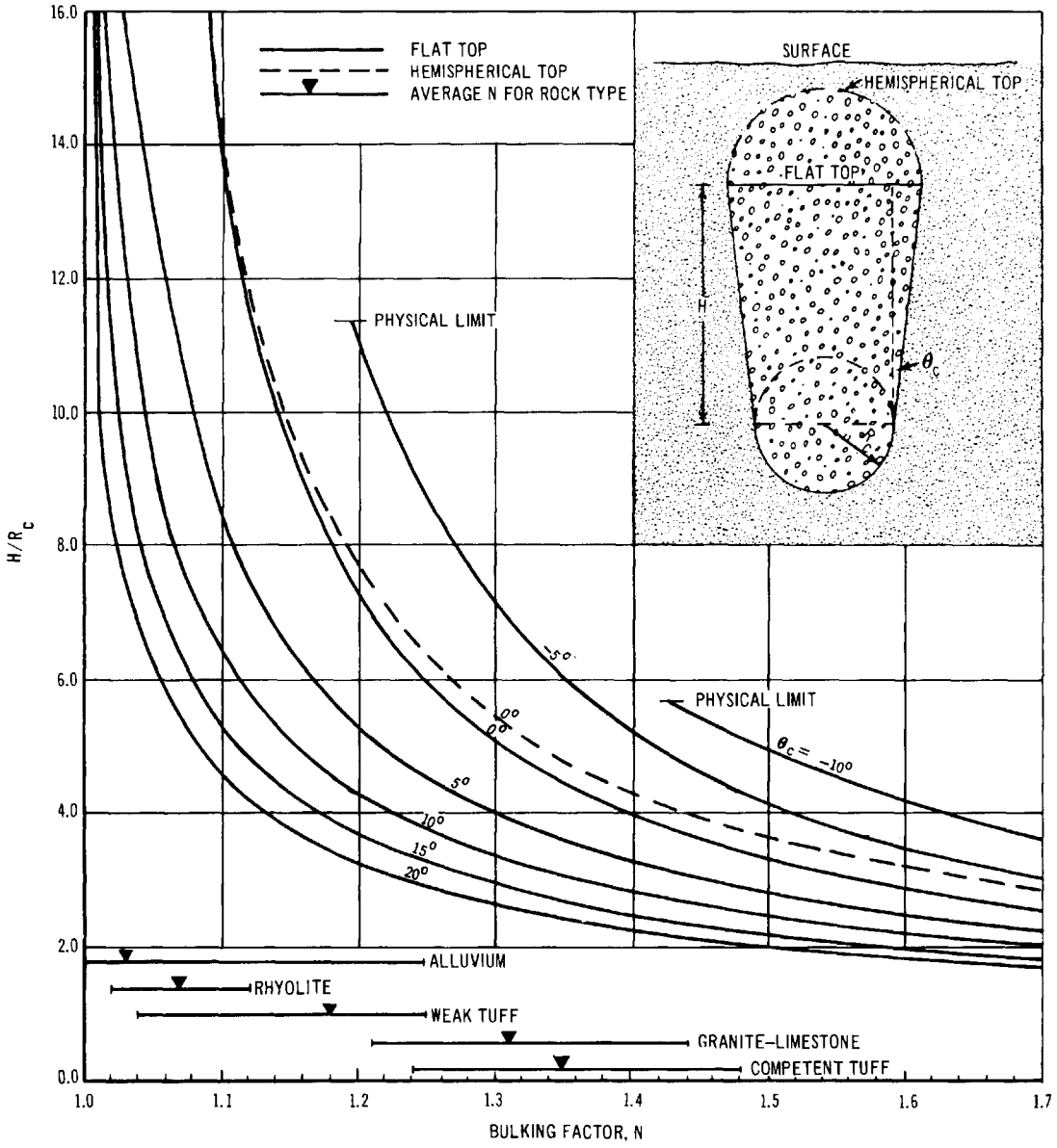

FIGURE 6. DIMENSIONLESS CHIMNEY HEIGHT AS A FUNCTION OF THE BULKING FACTOR

to the large fragments that are produced upon fracturing, resulting in a large percentage increase in the voids. Soils, on the other hand, have relatively lower bulking factors.

Graphical solutions of equation (33) are given in Figure 6. It can be seen that it is essential that an accurate value of N be found if the prediction of the chimney height for the excessive bulking condition is to be successful.

COMPARISON OF SUBSIDENCE AT THE NEVADA TEST SITE (NTS) WITH THEORY

A large number of contained underground nuclear detonation experiments have been conducted in the various test areas at the Nevada Test Site (NTS). Many of the explosions have produced subsidence craters, for which the cavity radius, and the radius, depth, volume, and time to collapse of the subsidence craters have been recorded. This information was compared with the theoretical principles discussed in the preceding sections. The assumed simplified geometry of a subsidence crater is shown in Figure 7. Very limited data are available for chimneys that do not reach the surface.

Subsidence Crater Radii

With the assumption of a conical-shaped chimney, the measured crater radius (R_{cr}) and cavity radius (R_c) can be used to compute the slope angle, (θ_c).

$$\tan \theta_c = \frac{R_{cr} - R_c}{DOB} \quad . \tag{36}$$

The procedures used in determining R_{cr} and R_c are given by Hakala.* Experimental verification of at least one conical-shaped chimney was found by Rawson and Rohrer.*

Values of θ_c obtained by equation (36) are plotted against the cavity radius in areas 2, 3, 9, and 10 at NTS in Figure 8. For classification purposes, the cavity radii have been reduced to dimensionless numbers. It appears that a tendency for piping (i.e., $\theta_c \approx 0^\circ$) exists for cavity radii less than about 1.0. For several events, θ_c is less than zero degrees. Numerous events with

*This work is contained in a classified report to the U.S. Atomic Energy Commission and is available to those with the proper access clearance and a need to know.

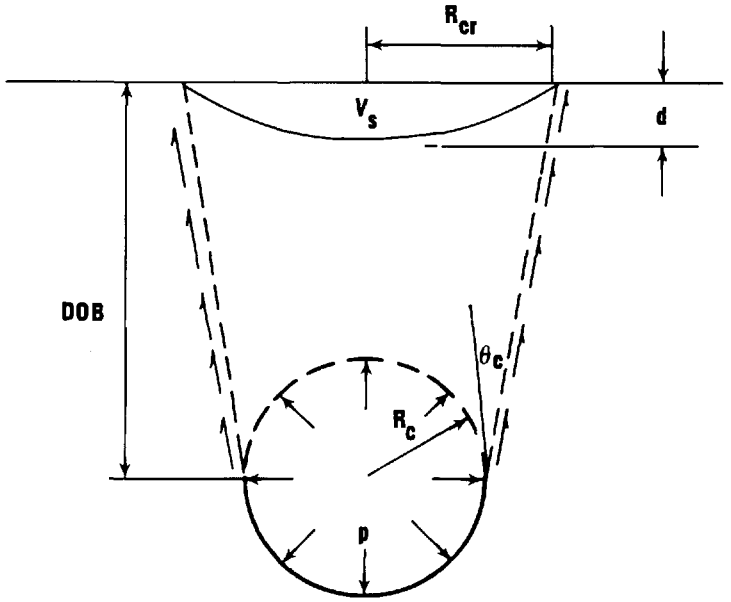

FIGURE 7. SUBSIDENCE CRATER GEOMETRY

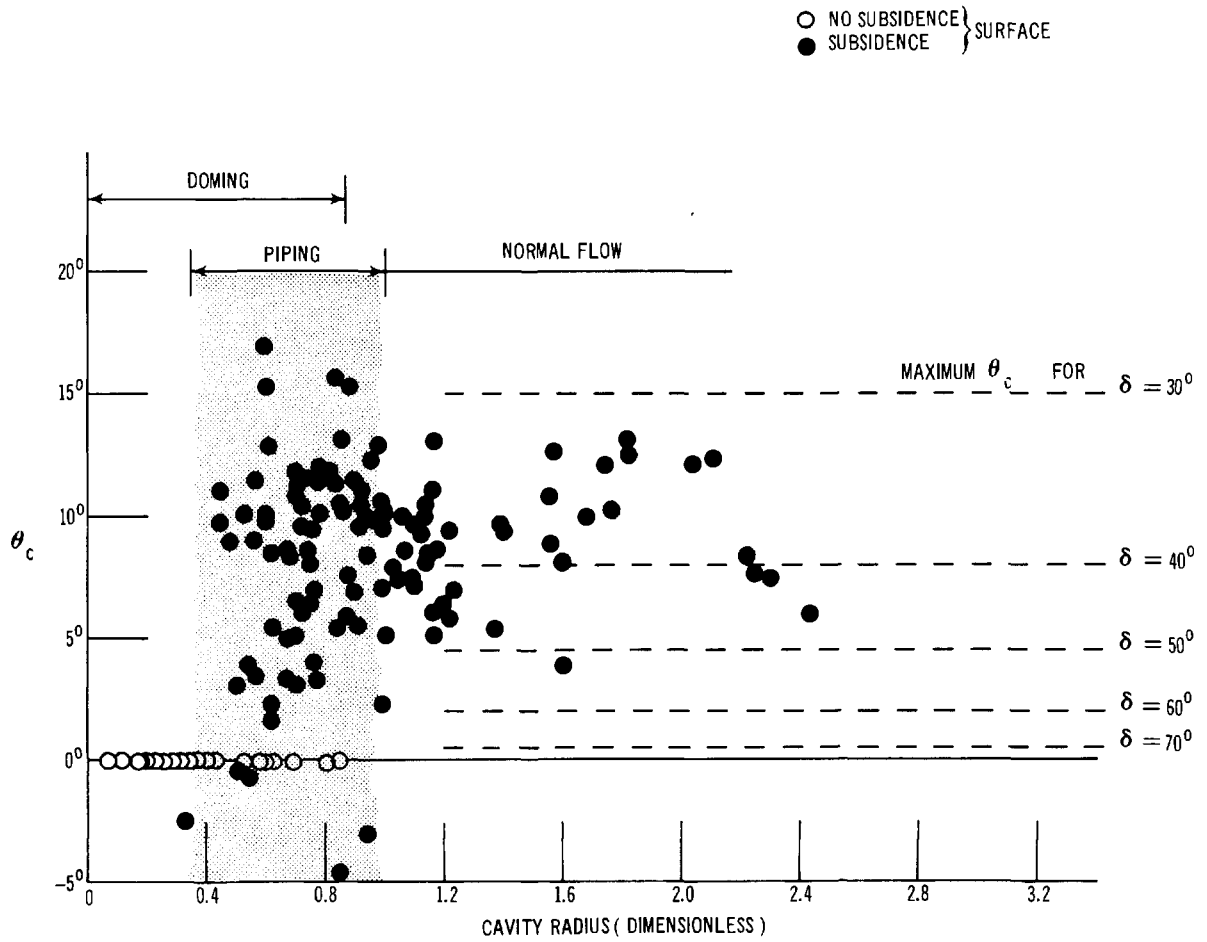

FIGURE 8 ANGLES OF FLOW CHANNEL (θ_c) vs CAVITY RADII IN ALLUVIUM IN AREAS 2, 3, 9, AND 10.

cavity radii less than about 0.6 (in all test areas) produce no surface subsidence, indicating the possibility of doming.

Approximate values of unconfined compressive strengths (C_o), as obtained from equations (30) and (32), are reasonable for the media being considered. A few observations of θ_c in rocks (not shown in Figure 8) indicate larger cavity radii at which piping results, which is to be expected for higher strength materials.

The scatter in Figure 8 is probably due to variations in the effective angle of friction, δ. However, almost all quantities lie within the theoretically predicted values for a normal range of δ(i.e., 30°-70°), and all slope angles θ_c are less than 17°. There is a predominance of data points between $\delta = 30°$ to 40°. This is less than the most common value of 50° observed for commercially handled materials (Johanson, 1964). [Jenike (1969) has recently found that the maximum slope angle for conical flow given in Table I can be exceeded for certain stress fields. Also, if the lower boundaries of the flow channel exceed the diameter of the cavity, this would appear in Figure 8 as larger θ_c's for the smaller radii (since smaller radii are usually associated with shallow depths.)]

Assuming no doming or piping, if the value of δ is known, the slope angle (θ_c) can be found from Table I. The crater radius can then be predicted from (assuming R_c can be accurately predicted):

$$R_{cr} = R_c + DOB \tan \theta_c \qquad (37)$$

Subsidence Crater Volumes

It was shown by Berry and Hakala* that the volume of a subsidence crater, V_{cr}, can be determined from

$$V_{cr} = \frac{2\pi}{3} DOB^3(N + 1)\left(\frac{R_c}{DOB}\right)^3 - \frac{\pi}{3} DOB^3(N - 1)$$

$$\left[3\left(\frac{R_c}{DOB}\right)^2 + \tan^2 \theta_c\left(\frac{R_c}{DOB}\right) + \tan^2 \theta_c\right] , \qquad (38)$$

$$(V_{cr} \geq 0) ,$$

*This work is contained in a classified report to the U. S. Atomic Energy Commission and is available to those with the proper access clearance and a need to know.

which is based upon an assumed conical chimney above the cavity. Graphical solutions of Equation (38) are given in Figures 9 through 11. It is obvious from these curves that the crater volumes are very sensitive to the bulking factor, N, and to the angle of the flow channel, θ_c. These parameters, in turn, are functions of the material properties.

Berry and Hakala* used the measured values of V_{cr} and θ_c and relation (38) to evaluate bulking factors for the various test areas. The results are plotted in Figure 12 as a function of a dimensionless cavity radius. Figure 12 indicates that the computed bulking factor decreases with increasing cavity radius, approaching an asymptotic value of about unity at a cavity radius of approximately 1.0. (Bulking factors less than unity are unlikely in dense materials. Errors in volumes of craters, cavity radii, etc, would contribute to the scatter.)

A flow channel having $\theta_c = 0°$ is the boundary between converging and diverging flow. Because there is a tendency for the intermediate principal stress (σ_α) to fluctuate between σ_1 and σ_3 under these conditions [see equations (6)], the flow is erratic and unsteady. This could produce variations in the bulking factors and, in general, give larger bulking factors. A cavity radius of about 1.0 does seem to agree with the upper limit of piping in Figure 8.

Subsidence Crater Depths

If the shape of the profile of a subsidence crater is known, the maximum depth of the crater, d, can be determined from a knowledge of the volume (V_{cr}) and the radius (R_{cr}).

For radial flow, Jenike (1961) found that the velocity u_r in an incompressible medium under axially symmetric conditions was

$$u_r = u_r^{\circ} \; e^{-3\int_{\sigma}^{\theta} \tan 2\eta \, d\theta} \quad , \qquad (39)$$

where u_r° is the velocity along the axis of symmetry. Although the velocity field may not be unique, Equation (39) indicates that the radial velocity decreases from the axis of symmetry

*This work is contained in a classified report to the U. S. Atomic Energy Commission and is available to those with the proper access clearance and a need to know.

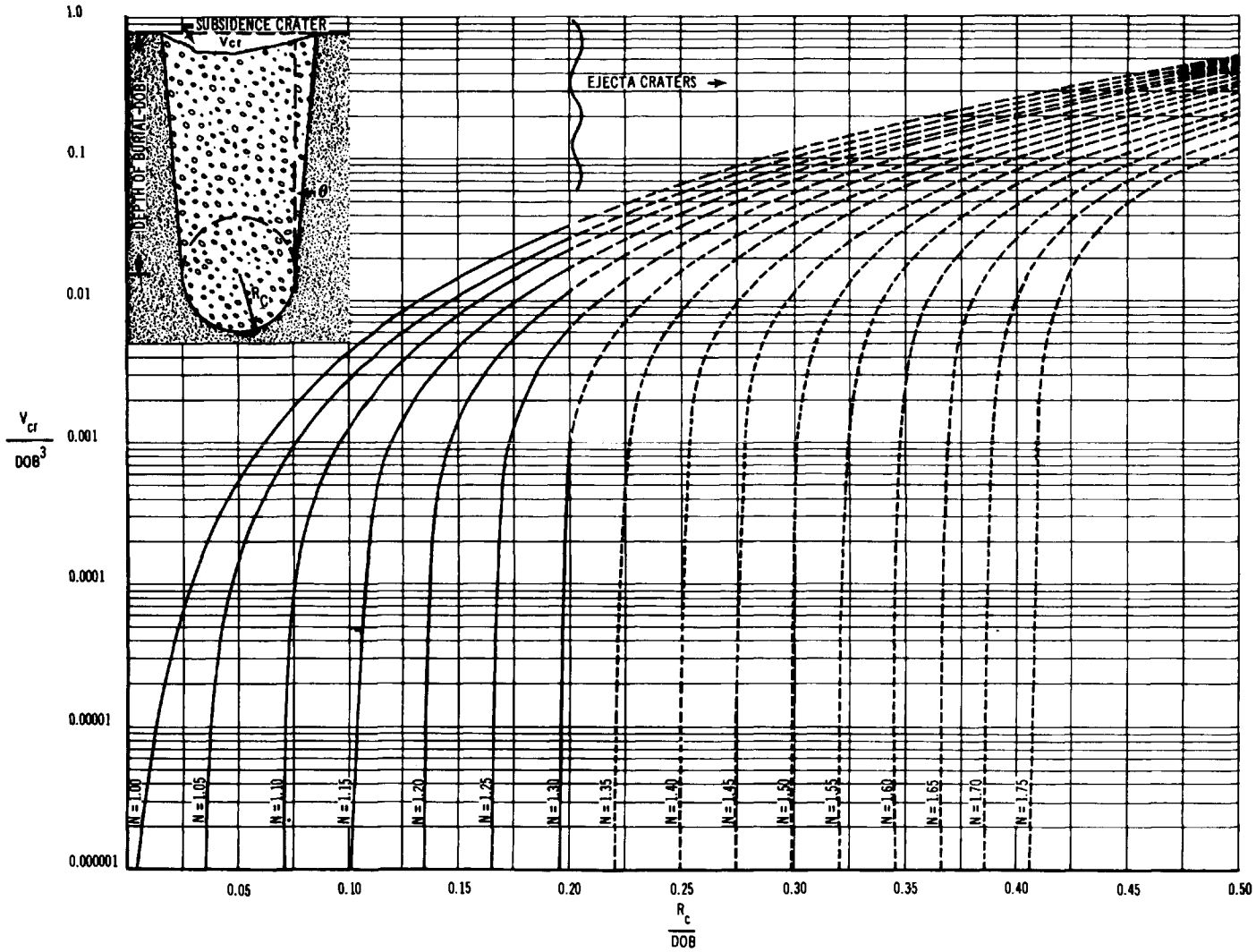

FIGURE 9. DIMENSIONLESS PLOT OF SUBSIDENCE CRATER VOLUMES ($\theta c = 0°$)

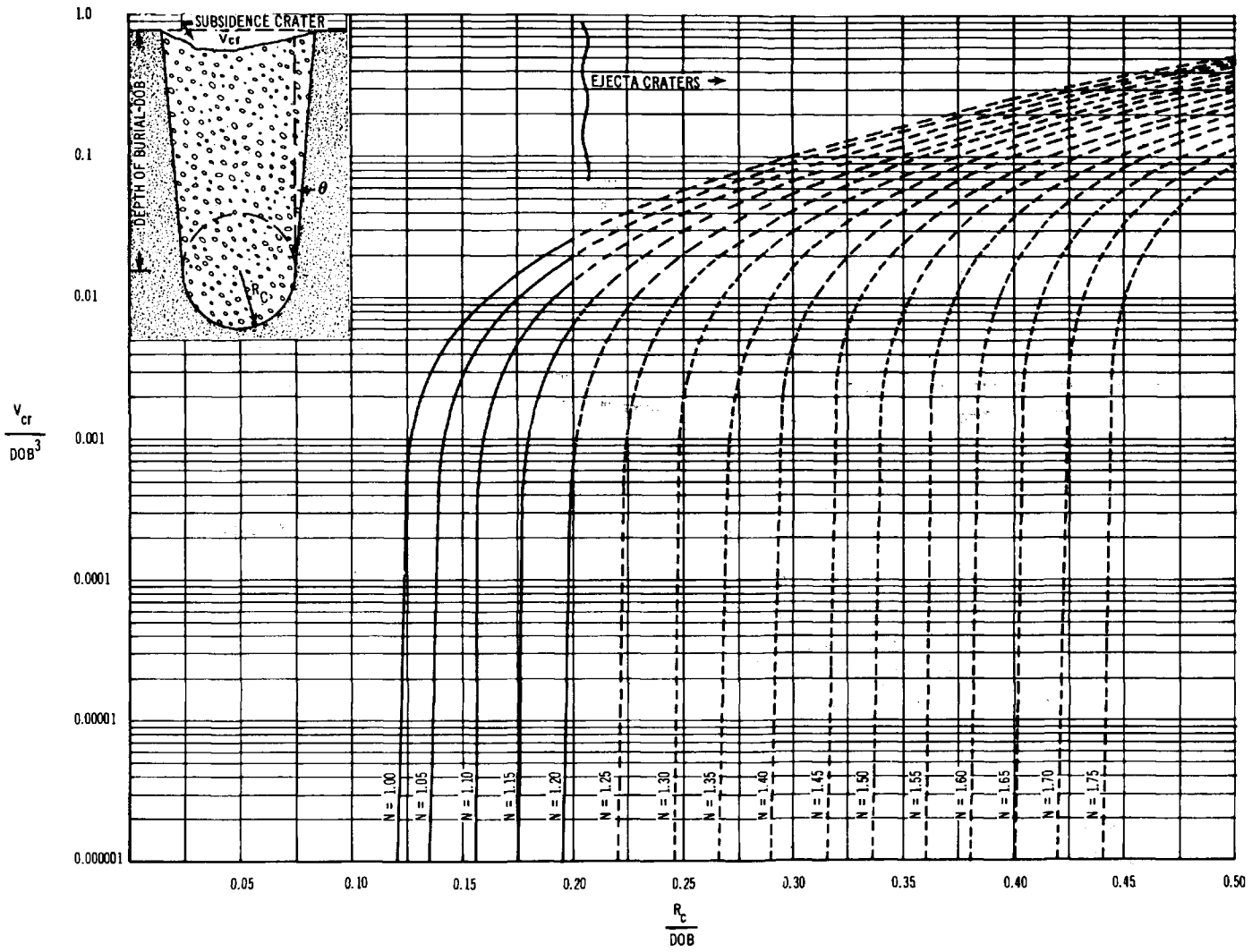

FIGURE 10. DIMENSIONLESS PLOT OF SUBSIDENCE CRATER VOLUMES ($\theta c = 5°$)

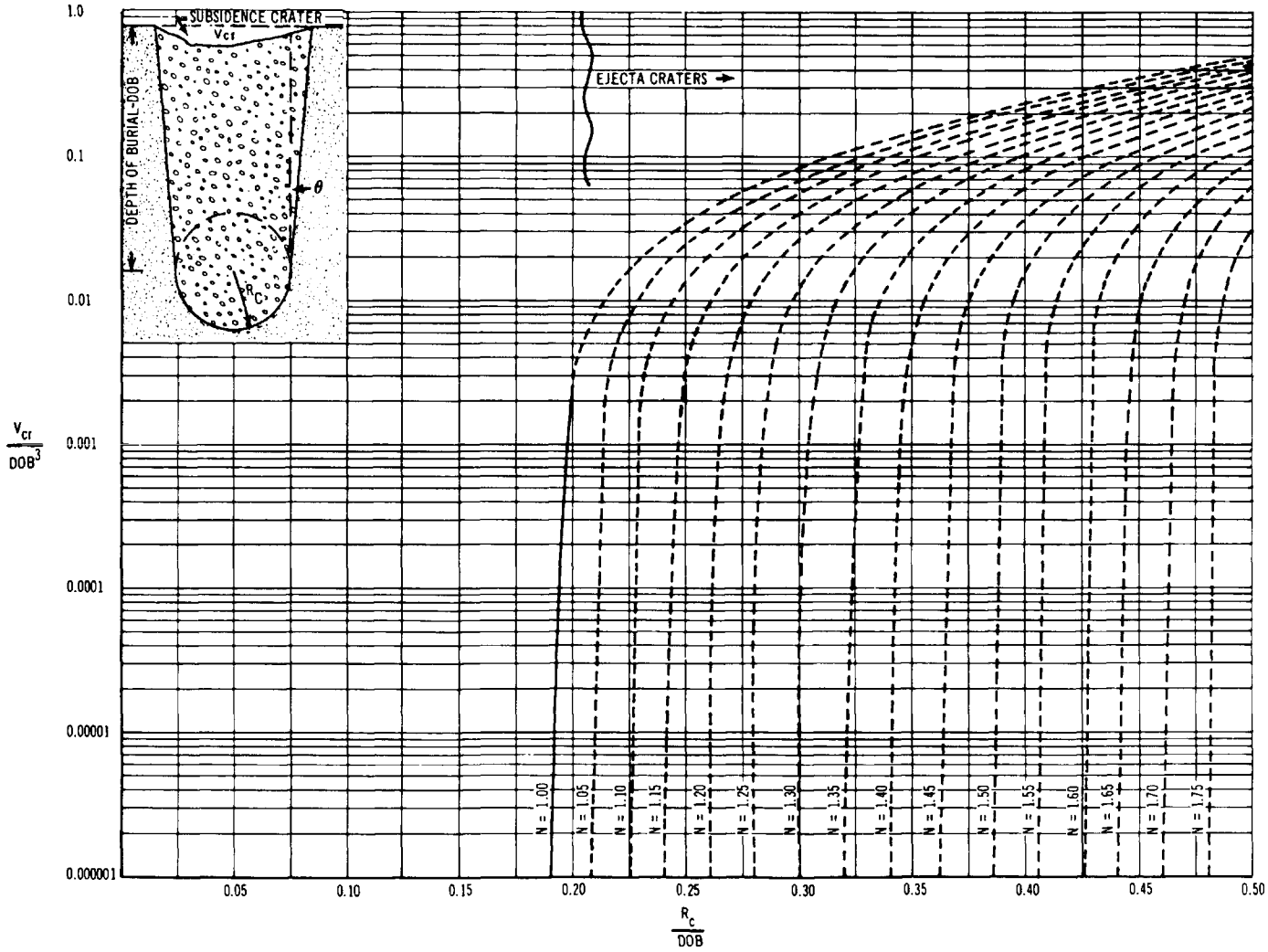

FIGURE 11. DIMENSIONLESS PLOT OF SUBSIDENCE CRATER VOLUMES ($\theta c = 10^0$)

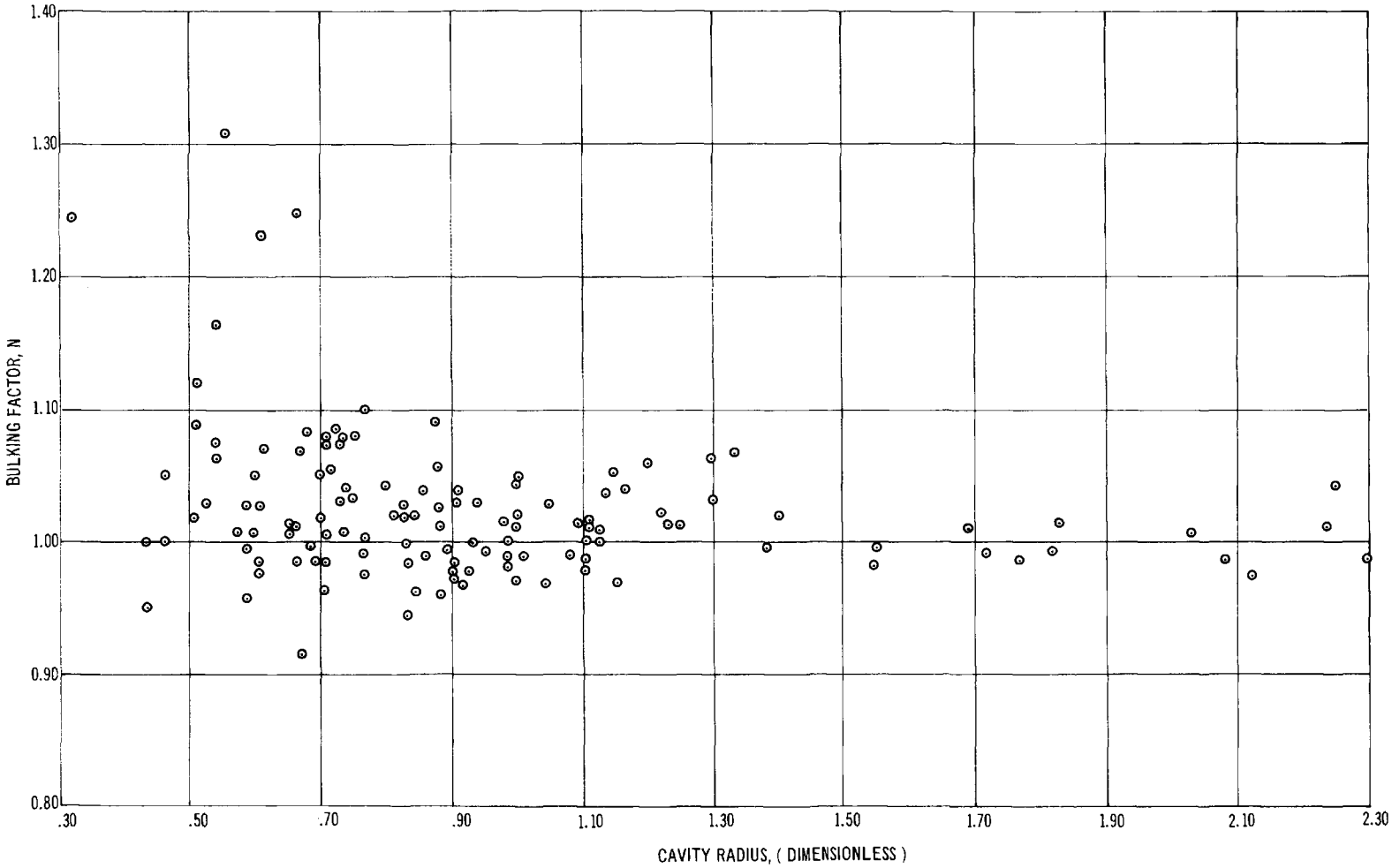

FIGURE 12. BULKING FACTORS FOR CHIMNEYS IN ALLUVIUM, AREAS 2, 3, 9, AND 10, NTS

toward the walls of the flow channel. (Cases do exist where a cylinder of material drops intact as a "plug.")

An approximate value for the maximum crater depth can be found from the relation:

$$d = \frac{m\ V_{cr}}{\pi\ R_{cr}^2} \quad , \tag{40}$$

where $V_{cr} = V_{cr}\ (DOB,\ R_c,\ \theta_c,\ N)$, $R_{cr} = R_{cr}\ (DOB,\ R_c,\ \theta_c)$, and m is a shape factor defining the profile. Restricting the crater profile to be concave upward, m can vary within the range, $1 < m < 3$ (for a cylinder, $m = 1$; paraboloid, $m = 2$; cone, $m = 3$). For craters at the Nevada Test Site, it has been found that m decreases with increasing depths of burial (DOB) (Hakala, 1968).* [Using a stochastic model, Sweet and Bogdanoff (1965) determined that the profile for a small subsidence should be V-shaped in a dimensional model of a cohesionless soil, which was verified in laboratory tests.]

Substituting equations (37) and (38) into (40) gives

$$d = \frac{m\ DOB}{3\left[\frac{R_c}{DOB} + \tan\theta_c\right]^2} \left\{ 2(N+1)\left(\frac{R_c}{DOB}\right)^3 - 3(N-1)\left(\frac{R_c}{DOB}\right)^2 \right.$$

$$\left. -2(N-1)\tan\theta_c\left(\frac{R_c}{DOB}\right) - (N-1)\tan^2\theta_c \right\} \quad , \tag{41}$$

$$(d \geq 0) \quad .$$

If the cavity radius is large enough to prevent piping, and $R_c/DOB \approx \tan\theta_c$, then for this case

$$d = \frac{m\ DOB}{12}\left\{ 2(N+1)\left(\frac{R_c}{DOB}\right) - 6(N-1) \right\} \quad . \tag{42}$$

Making the additional assumption that the bulking factor (N) is near unity,

$$d \cong \frac{m}{3}\ (R_c) \quad . \tag{43}$$

*This work is contained in a classified report to the U.S. Atomic Energy Commission and is available to those with the proper access clearance and a need to know.

Thus, the crater depth for low-bulking materials should lie in the range

$$\frac{1}{3} R_c < d < R_c \quad . \tag{44}$$

For craters that are concave upward, relation (44) has been verified (Hakala*).

Collapse Times

As discussed earlier, flow in vertical or nearly vertical channels is erratic because of the fluctuation of the circumferential stress. Jenike (1961) has also shown that zones of zero velocity are possible in steep flow channels if the velocity characteristics and sliplines do not coincide. It would then be anticipated that collapse times associated with subsidence in axially symmetric flow would be subject to large variations.

Approximate analyses by Hakala* have also shown the extreme sensitivity of the collapse time to the physical and mechanical properties of the medium. These analyses show that for a given scaled burial depth the time to collapse should increase with the size of the cavity. Although large deviations from a mean curve were found, there is a general increase in the collapse time as the cavity radius, yield of the explosion, and the depth of burial increases. (In general, all three of these parameters increase simultaneously.)

CONCLUSIONS

The subsidence associated with the collapse of an underground spherical cavity has been considered. Although the subsidence for many events has been controlled by geologic imperfections (faults, lineaments, etc.), most of the subsidence at NTS involves axially-symmetric conditions.

The fundamental equations and many of the concepts from bin-flow theory are applicable to the subsidence problem considered here. However, a knowledge of the strength properties, flow properties, and bulking characteristics is essential for the accurate prediction of subsidence values.

*This work is contained in a classified report to the U.S. Atomic Energy Commission and is available to those with the proper access clearance and a need to know.

REFERENCES

Jenike, A. W., and Shield, R. T., "On the Plastic Flow of Coulomb Solids Beyond Original Failure," J. of Appl. Mech., V. 26, Trans. ASME, V. 81, Series E, December 1959, pp. 599-602.

Jenike, A. W., Elsey, P. J., and Woolley, R. H., "Flow Properties of Bulk Solids," Proc. ASTM, 60, 1960, pp. 1168-1181.

Jenike, A. W., "Gravity Flow of Bulk Solids," Bull. No. 108, Utah Engineering Experiment Station, October 1961.

Jenike, Andrew W., and Yen, Bing Chen, "Slope Stability in Axial Symmetry," Proc. 5th Symp. on Rock Mech., Univ. of Minnesota, May, 1962, pp. 689-711.

Jenike, Andrew W., and Leser, Tadeusz, "A Flow- No-Flow Criterion in the Gravity Flow of Powders in Converging Channels," 4th Int. Conf. Congress on Rheology, Brown Univ., August 1963, pp. 125-141.

Jenike, Andrew W., Personal Communication, January 22, 1969.

Johanson, J. R., "Stress and Velocity Fields in the Gravity Flow of Bulk Solids," J. of Appl. Mech., V. 31, Trans. ASME, V. 86, Series E., September 1964, pp. 499-506.

Sokolnikoff, I. S., "Mathematical Theory of Elasticity," 2nd Edition, McGraw-Hill Book Company, Inc., 1956.

Sokolovski, V. V., Statics of Soil Media, Butterworth's Scientific Publications, London, 1960.

Sweet, Arnold L. and Bogdanoff, John L., "Stochastic Model for Predicting Subsidence," J. of the Engr. Mech. Div., ASCE, Vol. 91, No. EM2, Part 1, April, 1965, pp. 21-45.